ISPRS Journal of Photogrammetry and Remote Sensing 64 (2009) 259–266

Contents lists available at ScienceDirect

ISPRS Journal of Photogrammetry and Remote Sensing

journal homepage: www.elsevier.com/locate/isprsjprs

Validation of geometric models for fisheye lenses

D. Schneider *, E. Schwalbe, H.-G. Maas

Institute of Photogrammetry and Remote Sensing, Technische Universität Dresden, Helmholtzstraße 10, 01069 Dresden, Germany

ARTICLE INFO

Article history:
Received 4 March 2008
Received in revised form
31 December 2008
Accepted 8 January 2009
Available online 11 February 2009

Keywords:
Fisheye lens
Geometric modelling
Calibration
Bundle adjustment

ABSTRACT

The paper focuses on the photogrammetric investigation of geometric models for different types of optical fisheye constructions (equidistant, equisolid-angle, sterographic and orthographic projection). These models were implemented and thoroughly tested in a spatial resection and a self-calibrating bundle adjustment. For this purpose, fisheye images were taken with a Nikkor 8 mm fisheye lens on a Kodak DSC 14n Pro digital camera in a hemispherical calibration room. Both, the spatial resection and the bundle adjustment resulted in a standard deviation of unit weight of 1/10 pixel with a suitable set of simultaneous calibration parameters introduced into the camera model. The camera-lens combination was treated with all of the four basic models mentioned above. Using the same set of additional lens distortion parameters, the differences between the models can largely be compensated, delivering almost the same precision parameters. The relative object space precision obtained from the bundle adjustment was ca. 1:10 000 of the object dimensions. This value can be considered as a very satisfying result, as fisheye images generally have a lower geometric resolution as a consequence of their large field of view and also have a inferior imaging quality in comparison to most central perspective lenses.

1. Introduction

Area sensor cameras are usually characterized by central perspective geometry. This cannot be applied for the use of fisheye lenses (Fig. 1, left). Fisheye lenses are lenses with an extremely short focal length and a very wide field of view close to 180° or even beyond. Thus, one single fisheye image can represent a large part of the surroundings (Fig. 1, right). Images taken with a fisheye lens allowing for a field of view of 180° are also called hemispherical images. As this geometry cannot be described with the geometry of central perspective projection, it is necessary to apply a separate geometric model for the use of fisheye images in photogrammetric applications. In Section 2, four different geometric models, which have been used for fisheye camera modeling and which are known from the literature (e.g. Ray (1994), Abraham and Förstner (2005) and Kannala and Brandt (2006)), are described. The models are extended by a set of additional parameters to account for deviations from the camera model. The main part of this paper is the validation of the geometric models, implemented in a spatial resection and a photogrammetric self-calibrating bundle adjustment, which is outlined in Section 3.

Cameras with fisheye lenses have also been called 'pseudo panoramic cameras' in literature (Schröder, 1981; Regensburger, 1990). The fisheye image is characterized by the fact, that lines which do not pass through the center of the image, are strongly bent. Fisheye lenses owe their name to this effect, since it corresponds to the view of a fish, which is looking through the water surface.

Fisheye lenses have opened up numerous (non-photogrammetric) applications due to their wide field of view. For example they are used for surveillance applications (e.g. in public buildings or public transport vehicles), for recording of overview images (e.g. interiors or street scenes) or within the effect photography. Frequently, fisheye images are presented in the internet. For this purpose the images are often projected onto a cylinder surface (Luhmann, 2004) in order to obtain 360° images, which can be viewed interactively with common panoramic viewer software such as Apple's QuickTime VR software.

In comparison to 'real panoramic cameras' captured with a rotating linear sensor as described in Schneider and Maas (2006) and Amiri Parian (2007) fisheye lenses come at a low cost, because they can be combined with conventional cameras with array sensors. A rather important advantage with respect to panoramic cameras is the fact that they can be used for recording moving objects, as they are snap-shot cameras. Disadvantages can be seen in the lower resolution obtained by imaging a wide field of view onto a limited sensor format, and in a usually inferior imaging quality. In particular, the strong chromatic aberration has a negative effect on the image quality of color images. However, approaches have been developed for the correction of this effect (Luhmann et al., 2006; Schwalbe and Maas, 2006; van den Heuvel et al., 2006).

* Corresponding author. Tel.: +49 351 463 33144; fax: +49 351 463 37266.
E-mail addresses: danilo.schneider@tu-dresden.de (D. Schneider), ellen.schwalbe@tu-dresden.de (E. Schwalbe), hans-gerd.maas@tu-dresden.de (H.-G. Maas).

0924-2716/$ – see front matter
doi:10.1016/j.isprsjprs.2009.01.001

Fig. 1. Fisheye lens Nikkor 8 mm (left), Fisheye image (right).

Fisheye cameras are also increasingly being used for photogrammetric measurement tasks, for instance for the three-dimensional modeling of interiors. In Beers (1997) the applications of a fisheye camera system (CycloMedia Mapper), mounted on top of a car, for city scene capture is reported. Moreover, fisheye lenses are frequently being used in forest science applications, e.g. for the quantitative assessment of the illumination conditions of young plants (Wagner, 1998; Schwalbe et al., 2006). For this purpose, the imaging axis is set vertically upwards within the forest. Subsequently, radiation relevant areas of the canopy are segmented in the appropriate images in order to derive quantitative values for the direct sun radiation on the image position.

Fisheye lenses can be also combined with rotating linear array cameras in order to achieve an image with a full spherical field of view (Bonnet, 2004). The combination of the equidistant geometric fisheye model and the geometric model for rotating linear array cameras has already successfully been tested in Schneider and Schwalbe (2005).

Manufacturers of terrestrial laser scanners often combine their devices with digital cameras. Some terrestrial laser scanners have an almost full spherical field of view. Covering this field of view with a conventional central perspective camera requires a large number of images. Using a fisheye-camera allows to reduce the number of images drastically. The images are mainly used to colorize laser scanner point clouds, to texturize 3D models generated from the laser scanner data or to produce orthophotos (e.g. in architectural applications).

All these photogrammetric applications of fisheye lenses require a camera and lens calibration based on a precise geometric model to achieve accurate results. Calibration procedures for fisheye lenses are published for example in Schwalbe (2005) and Kannala and Brandt (2006). Furthermore (Orekhov et al., 2007) suggests a calibration method with the automatic selection of the distortion model.

The geometric fisheye models can also be used to convert parts of a hemispherical image into a central perspective view to be used in photogrammetric standard software. This can be carried out by the mathematical definition of a tangential plane on an arbitrary position of the 'fisheye hemisphere' and the subsequent projection of the image content on this plane, for instance by an indirect rectification method.

2. Geometric models for fisheye lenses

2.1. Fisheye lenses

Fisheye lenses can be categorized by the size of the image circle diameter in relation to the image or sensor format. They can be differentiated into circular image fisheye lenses or full format fisheye lenses. The image circle of a circular fisheye will be completely inside the image sensor format, i.e. the image circle diameter corresponds to the shorter edge of the sensor format.

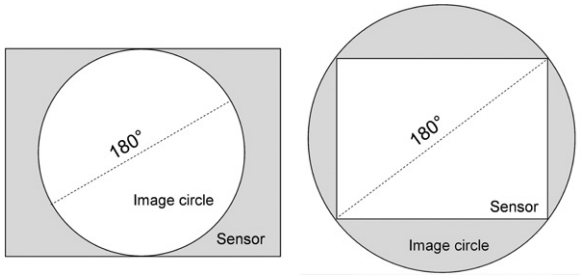

Fig. 2. Circular 180° fisheye (left), diagonal 180° fisheye (right).

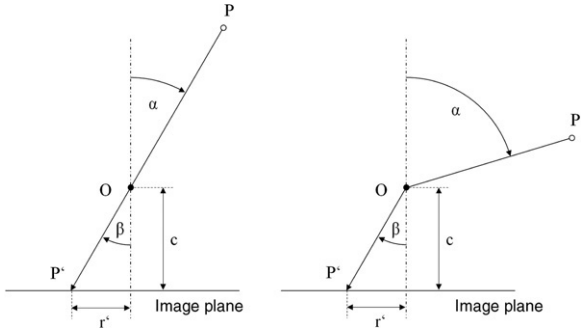

Fig. 3. Undistorted central perspective geometry (left) vs. fisheye projection geometry (right).

Thus, some areas of the sensor are not utilized (Fig. 2, left). The image circle diameter of a full format fisheye lens corresponds to the diagonal of the sensor format, therefore it is also called diagonal fisheye. However, the maximum field of view of the fisheye lens can only be reached in the image diagonal (Fig. 2, right). In addition to the fisheye lenses, there are also fisheye converters for conventional lenses available. The modeling and calibration of such a converter lens is described for example in Bakstein and Pajdla (2002).

Fisheye lenses can also be classified by their projection geometry, which depends on the construction of the lens. There are lenses with an equidistant, equisolid-angle and orthographic projection (Prenzel, 1986; Ray, 1994). The appropriate geometric models will be described in detail in Section 3. The technical construction of most fisheye lenses complies with the equidistant or equisolid-angle projection. Diagonal fisheye lenses are mainly constructed following the equisolid-angle projection geometry, where the distortion in the image edges is more significant in comparison to fisheye lenses with the equidistant projection. The orthographic projection geometry can only be realized with a sophisticated optical construction. There are other types of projection, which are not practically realizable, as for example the stereographic projection geometry (Ray, 1994).

In the following, the fundamental geometric models for the different construction principles of fisheye lenses are shown (Abraham and Förstner, 2005; Kannala and Brandt, 2006). The models are extended by a set of additional parameters to compensate for lens errors and deviations from the ideal model.

2.2. Types of fisheye projection

Fig. 3 shows a typical fisheye projection in comparison to the central perspective projection.

The projection rays of the central perspective projection are straight lines and intersect in the projection center.

The following relation between incidence angle α and reflection angle β can be applied, where r' is the image radius and c the principal distance:

$$\alpha = \beta \qquad r' = c \cdot \tan\alpha. \tag{1}$$

In contrast to central perspective projection a ray's incidence angle α is different from its accordant reflection angle β in all fisheye projections. The rays are refracted in the direction of the optical axis. In the following, different types of fisheye projections are introduced:

Equidistant projection:

$$\alpha \neq \beta \qquad r' = c \cdot \alpha. \tag{2}$$

The angles of incidence are translated linearly into radial distances within the image. Therefore, this projection allows for the measurement of angles in radial direction (e.g. celestial images).

Equisolid-angle projection:

$$\alpha \neq \beta \qquad r' = 2c \cdot \sin\frac{\alpha}{2}. \tag{3}$$

This projection type can also be called equal-area projection. This means that the ratio of an incident solid angle and its resulting area in the image is constant. Thus, such lenses are particularly suitable to measure cover areas (e.g. canopy cover images or cloud cover images).

Orthographic projection:

$$\alpha \neq \beta \qquad r' = c \cdot \sin\alpha. \tag{4}$$

For this projection type the radial distance in the image is proportional to the sinus of the angle of incidence. In this way an orthogonal projection of the hemisphere onto the image plane is realized, though this leads to a strong distortion at the margin of the image.

Stereographic projection:

$$\alpha \neq \beta \qquad r' = 2c \cdot \tan\frac{\alpha}{2}. \tag{5}$$

This projection type is an equal-angle projection. This means that an angle in object space and its corresponding angle in the image are identical. In this way proportions of objects will remain unchanged using this projection.

2.3. Model equations

To describe the projection of an object point into a hemispherical fisheye lens image, three coordinate systems are used: The superordinated Cartesian object coordinate system (X, Y, Z) and the camera coordinate system (x, y, z) (see Fig. 4). The image coordinate system (x', y') is defined as usual in photogrammetric applications, which means the origin is the image center, and the x'- and y'-axes are parallel with the x- and y-axes of the camera coordinate system.

Object coordinates are transformed into the camera coordinate system using Eq. (6), where $\mathbf{X}$ is the coordinate vector in the object coordinate system, $\mathbf{x}$ the coordinate vector in the camera coordinate system, $\mathbf{R}$ the rotation matrix and $\mathbf{X}_0$ the translation between object and camera coordinate system:

$$\mathbf{x} = \mathbf{R}^{-1}(\mathbf{X} - \mathbf{X}_0). \tag{6}$$

The incidence angle α in the camera coordinate system is defined as follows:

$$\tan\alpha = \frac{\sqrt{x^2 + y^2}}{z}. \tag{7}$$

For the different equations for fisheye projection as described above, the image radius r' is defined as a function of the incidence angle α and the principle distance (Eqs. (1)–(5)). Instead of functions for the image radius r', functions for the image coordinates x' and y' are required. For this purpose Eq. (8) is applied:

$$r' = \sqrt{x'^2 + y'^2}. \tag{8}$$

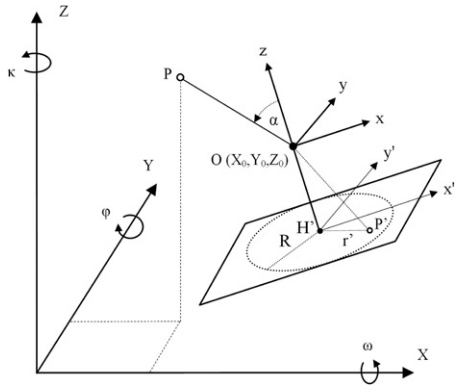

Fig. 4. Geometrical model of a fisheye camera.

To describe the image coordinates x' and y' as a function of the object point coordinates in the camera coordinate system x and y Eq. (9) has to be introduced. This equation is set up applying the theorem on intersecting lines in the plane which is defined by the z-axis, the image point and the object point.

$$\frac{x'}{y'} = \frac{x}{y}. \tag{9}$$

After transforming equations (8) and (9), the projection equations become:

$$x' = \frac{r'}{\sqrt{\left(\frac{y}{x}\right)^2 + 1}} \qquad y' = \frac{r'}{\sqrt{\left(\frac{x}{y}\right)^2 + 1}}. \tag{10}$$

The insertion of these equations into the different types of projection (Eqs. (2)–(5)) leads to the respective geometric models of with fisheye lens cameras. The coordinates of the particular object point in the camera coordinate system x, y and z still have to be transformed into the object coordinate system using Eq. (6). The model equations are finally extended by the coordinates of the principle point x'_0 and y'_0 and the correction terms $\Delta x'$ and $\Delta y'$ which contain additional parameters to compensate for systematic effects (see Section 3.3).

Equidistant projection:

$$\begin{aligned} x' &= c \cdot \frac{\arctan\frac{\sqrt{x^2+y^2}}{z}}{\sqrt{\left(\frac{y}{x}\right)^2 + 1}} + x'_0 + \Delta x' \\ y' &= c \cdot \frac{\arctan\frac{\sqrt{x^2+y^2}}{z}}{\sqrt{\left(\frac{x}{y}\right)^2 + 1}} + y'_0 + \Delta y'. \end{aligned} \tag{11}$$

Equisolid-angle projection:

$$\begin{aligned} x' &= c \cdot \frac{\sin\left(\frac{1}{2} \cdot \arctan\frac{\sqrt{x^2+y^2}}{z}\right)}{\sqrt{\left(\frac{y}{x}\right)^2 + 1}} + x'_0 + \Delta x' \\ y' &= c \cdot \frac{\sin\left(\frac{1}{2} \cdot \arctan\frac{\sqrt{x^2+y^2}}{z}\right)}{\sqrt{\left(\frac{x}{y}\right)^2 + 1}} + y'_0 + \Delta y'. \end{aligned} \tag{12}$$

Orthographic projection:

$$x' = c \cdot \frac{\sin\left(\arctan\frac{\sqrt{x^2+y^2}}{z}\right)}{\sqrt{\left(\frac{y}{x}\right)^2+1}} + x'_0 + \Delta x'$$
$$y' = c \cdot \frac{\sin\left(\arctan\frac{\sqrt{x^2+y^2}}{z}\right)}{\sqrt{\left(\frac{x}{y}\right)^2+1}} + y'_0 + \Delta y'. \quad (13)$$

Stereographic projection:

$$x' = c \cdot \frac{\tan\left(\frac{1}{2}\cdot\arctan\frac{\sqrt{x^2+y^2}}{z}\right)}{\sqrt{\left(\frac{y}{x}\right)^2+1}} + x'_0 + \Delta x'$$
$$y' = c \cdot \frac{\tan\left(\frac{1}{2}\cdot\arctan\frac{\sqrt{x^2+y^2}}{z}\right)}{\sqrt{\left(\frac{x}{y}\right)^2+1}} + y'_0 + \Delta y'. \quad (14)$$

For the above mentioned equations the following exceptions have to be considered: In case of $x = 0$ the resulting image coordinate $x' = 0$ and in case of $y = 0$ the resulting image coordinate $y' = 0$.

2.4. Additional parameters

As additional parameters to compensate for deviations of the geometric fisheye model from the physical reality the same parameters are applied as they are in common use for central perspective lenses (Eqs. (15) and (16)). These are parameters to describe the radial symmetric distortion and the decentering distortion (Brown, 1971) as well as parameters to model affinity and shear (El-Hakim, 1986).

$$\Delta x = x' \cdot (A_1 r'^2 + A_2 r'^4 + A_3 r'^6) + B_1 \cdot (r'^2 + 2x'^2) + 2B_2 x'y' + C_1 \cdot x' + C_2 \cdot y' \quad (15)$$

$$\Delta y = y' \cdot (A_1 r'^2 + A_2 r'^4 + A_3 r'^6) + 2B_1 x'y' + B_2 \cdot (r'^2 + 2y'^2) \quad (16)$$

where

A_1, A_2, A_3 = radial distortion parameters

B_1, B_2 = decentering distortion parameters

C_1, C_2 = horizontal scale factor, shear factor.

The use of these additional parameters is well-established for the modeling of central perspective cameras with array sensors. In the investigations described in the paper the central perspective geometric model is substituted by the basic geometric fisheye model as described in the previous section, whereas the Brown-parameters are used for the compensation of remaining systematic effects. The paper does not aim for investigating different parameterization models. Extended parameterizations are described for example in Scaramuzza et al. (2006) and Frank et al. (2007), where additional parameters for misalignment and non-orthogonality of the image plane with respect to the optical axis are considered. Another example is given by Gennery (2006), where the modeling of the movement of the entrance pupil depending on the incidence angle is described, which can be particularly significant for fisheye lenses.

3. Validation

The fundamental fisheye lens camera models as shown above, extended by additional parameters for self-calibration, were implemented in a spatial resection and a bundle adjustment and tested in a specially arranged hemispheric camera calibration room. The module has also been implemented in a versatile bundle adjustment program for the simultaneous adjustment of central perspective, panoramic and hemispheric images together with terrestrial laser scanner measurements (Schneider and Schwalbe, 2008). The goal is to assess the accuracy potential of the used fisheye lens in photogrammetric standard methods considering the different fisheye projection models. It is expected, that there are differences in the suitability of the fisheye projection models. Although it is assumed that the use of fisheye lenses results in lower accuracies in comparison to conventional central perspective lenses, it should be possible to achieve sub-pixel accuracy.

3.1. Calibration room

For the analysis of the geometric models of fisheye lenses, a calibration room has been established which was designed to match the specific requirements of the calibration of fisheye lenses (Schwalbe, 2005). The size of the calibration room is about $4 \times 5 \times 3$ m^3. 141 control points are distributed in a way that they form concentric circles on the image plane of a hemispheric image taken from the center of the calibration room. The targets to signalize object points are mainly coded targets that can be identified automatically. Uncoded targets are merely used for points that are projected into the peripheral parts of the fisheye image, where coded targets can often not be identified reliably as a consequence of large image distortions. The reference coordinates have been determined with a standard deviation between 0.02 and 0.23 mm from a large number of central perspective images processed in the commercial photogrammetry system AICON 3D Studio. Fig. 5 shows an image of the calibration room taken from the center of the room with an upwards looking fisheye lens camera. Since it is not possible to apply a ring flash while taking fisheye images, retro reflecting targets could not be used. The illumination deficits had to be compensated by longer exposure times.

3.2. Data acquisition

For the verification of the geometric fisheye models, a digital 14 megapixel camera (Kodak DCS 14n Pro) has been used in combination with an 8 mm fisheye lens (Nikkor). Images taken using fisheye lenses often show strong effects of chromatic aberration. Thus, only the green channel of the calibration images has been used for further analysis. The chromatic aberration can be considered in the geometric model but this is not applied for the geometric models discussed here. An approach to determine and to eliminate effects of chromatic aberration by introducing partially independent parameter sets for the three color channels is e.g. described in Schwalbe and Maas (2006). The chromatic aberration has also been addressed by Luhmann et al. (2006) and van den Heuvel et al. (2006).

Sub-pixel accuracy measurements of target image coordinates in the hemispherical images were conducted using an off-the-shelf industrial photogrammetry system. For the analysis referring to the spatial resection, an image was used taken from the center of the calibration room (similar to Fig. 5) and the coordinates of 116 image points were measured and used for all calculation examples described below. The angle of incidence of these points varies from 0°–80°.

3.3. Spatial resection

3.3.1. Processing and results

For each of the geometric fisheye model described in Section 3, the calculation of the spatial resection has been conducted several times, successively introducing more additional parameters. Table 1 shows the standard deviation of unit weight for different calculation versions as a simple criterion for the evaluation of the

Table 1
Spatial resection results: standard deviation of unit weight $\hat{\sigma}_0$ in (pixel).

		Equi-distant model	Equisolid-angle model	Ortho-graphic model	Stereo-graphic model	Central persp. model
Exterior and interior orientation only	$X_0, Y_0, Z_0, \omega, \varphi, \kappa, c, x_0, y_0$	7.701	2.075	24.046	32.796	56.806
+ Rad.-sym. distortion	A_1, A_2, A_3	0.132	0.134	2.061	0.135	13.509
+ Decentering distortion	B_1, B_2	0.103	0.107	1.976	0.107	12.426
+ Affinity, Shear	C_1, C_2	0.102	0.106	1.969	0.107	12.459

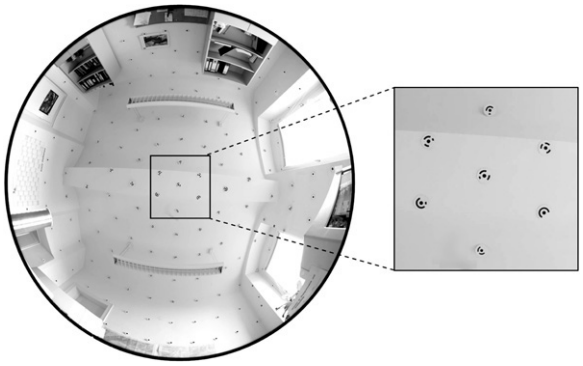

Fig. 5. Calibration room for fisheye lenses.

suitability of the geometric model for the camera-lens combination at hand.

Fisheye lenses mostly are constructed complying with the equidistant and equisolid-angle model and more rarely the orthographic model. Although the stereographic model is rather theoretical, it is also considered here for completeness. All calculations have also been conducted assuming a central perspective projection, although this is only possible for object points with incidence angles smaller than 90°. Table 1 (first row) shows that the basic model of equisolid-angle projection (without inner orientation and additional parameters) delivers the best precision (2 pixels in image space). As expected, the accuracy is worst applying the central perspective projection.

In case of the additional calculation of the parameters of radial symmetric distortion (Table 1, third row), the standard deviation of unit weight is almost identical for equidistant, equisolid-angle and stereographic model (0.13 pixels). It can be stated that the differences between the fundamental geometric models are almost fully compensated by the polynomial of radial symmetric distortion when applying these types of projections to the Nikkor lens. In Table 2 the values and related standard deviations for the parameters of exterior orientation, interior orientation and for radial symmetric distortion are listed for the equidistant and equisolid-angle model. Obviously, the distortion coefficients A_1 to A_3 vary strongly between the models. The exterior and interior orientation is not influenced using different fisheye projection models.

This different influence of the additional parameters is clearly visualized in Fig. 6, where the distortion curves for all models are shown. While the curve for the equisolid-angle model indicates only small corrections, all other curves show much higher values. The radius of the fisheye image on the sensor is 12 mm. At this position the distortion is 0.3 mm (35 pixels) for the equisolid-angle model, 0.9 mm (105 pixels) for the equidistant model, 2.3 mm (208 pixels) for the stereographic model and 3.8 mm (460 pixels) for the central perspective model. For the orthographic model the distortion at the margin of the image amounts to (theoretically) 70 mm. The standard deviation of unit weight after the integration of the distortion parameters still amounts 13 pixels for the central perspective model, whereas this value is only 0.13 pixels for equidistant, equisolid-angle and stereographic model (see Table 1).

Table 2
Spatial resection result: selection of estimated parameters.

	Equidistant model	Equisolid-angle model
X_0	3.0463 ± 0.0002 mm	3.0463 ± 0.0002 mm
Y_0	-0.1316 ± 0.0001 mm	-0.1316 ± 0.0001 mm
Z_0	-0.6837 ± 0.0003 mm	-0.6835 ± 0.0003 mm
ω_1	200.6830 ± 0.0045 gon	200.6833 ± 0.0046 gon
ϕ_2	-0.6845 ± 0.0055 gon	-0.6873 ± 0.0057 gon
κ_3	0.8486 ± 0.0016 gon	0.8486 ± 0.0017 gon
c	7.9978 ± 0.0014 mm	7.9983 ± 0.0015 mm
x_0	-0.1407 ± 0.0012 mm	-0.1411 ± 0.0012 mm
y_0	-0.0215 ± 0.0009 mm	-0.0214 ± 0.0010 mm
A_1	$(-6.244 \pm 0.057) \times 10^{-4}$	$(0.146 \pm 0.079) \times 10^{-4}$
A_2	$(1.497 \pm 0.089) \times 10^{-6}$	$(1.845 \pm 0.136) \times 10^{-6}$
A_3	$(-5.015 \pm 0.413) \times 10^{-9}$	$(-5.075 \pm 0.738) \times 10^{-9}$

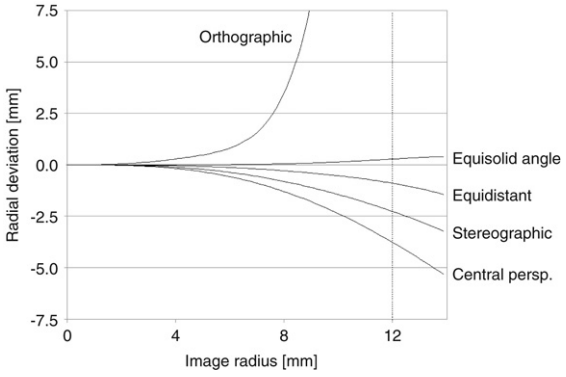

Fig. 6. Radial-symmetric distortion applying different geometric fisheye models.

The insertion of decentering distortion leads to a further improvement of ~20%, while further parameters (affinity and shear) yield only a marginal improvement (Table 1, last row).

The equidistant model in combination with the additional parameters delivers the best accuracy (standard deviation of unit weight: 0.102 pixels) for the specific camera + fisheye lens combination used in this test. Almost identical results could be obtained for the equisolid-angle model with the same parameter set (standard deviation of unit weight: 0.106 pixels), although this model shows much smaller additional parameter corrections.

Translating the standard deviation of 0.1 pixels from image space into object space, this corresponds to a lateral accuracy of 0.3 mm in a distance of 3 m (average distance to the object points in the calibration room). This means that remaining residuals (see Fig. 7) could already partly reflect the influence of the control point accuracy. This will to be verified in the following by applying a free network bundle adjustment.

3.4. Bundle adjustment

The spatial resection results will be verified in a bundle adjustment procedure with a total of nine images taken in the same calibration room. In particular, the question shall be answered, whether the calculation without any limitations caused by the accuracy of reference points leads to an improvement of the

Table 3
Bundle adjustment results applying basic geometric models.

	Standard deviation of unit weight $\hat{\sigma}_0$	RMS_X	RMS_Y	RMS_Z
Equidistant model	4.034 pixel	5.15 mm	5.57 mm	8.37 mm
Equisolid-angle model	1.304 pixel	1.66 mm	1.78 mm	2.71 mm
Orthographic model	19.036 pixel	23.28 mm	24.18 mm	38.72 mm
Stereographic model	13.455 pixel	17.31 mm	18.83 mm	26.81 mm
Central perspective model	38.635 pixel	44.25 mm	47.71 mm	64.11 mm

Table 4
Bundle adjustment results applying geometric models incl. additional parameters.

	Standard deviation of unit weight $\hat{\sigma}_0$	RMS_X	RMS_Y	RMS_Z
Equidistant model	0.280 pixel	0.37 mm	0.39 mm	0.51 mm
Equisolid-angle model	0.282 pixel	0.37 mm	0.39 mm	0.52 mm
Orthographic model	1.958 pixel	2.53 mm	2.70 mm	3.56 mm
Stereographic model	0.284 pixel	0.37 mm	0.40 mm	0.52 mm
Central perspective model	10.087 pixel	12.21 mm	13.05 mm	17.50 mm

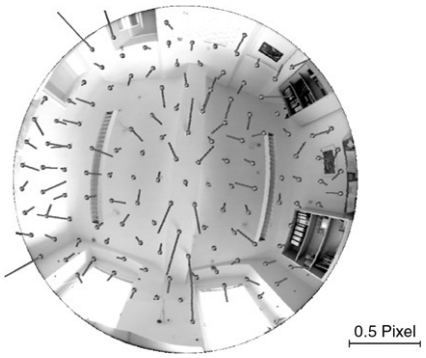

Fig. 7. Remaining residuals after the spatial resection with consideration of additional parameters.

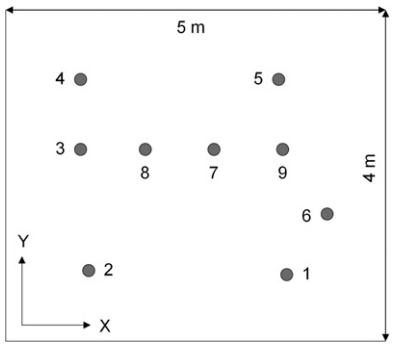

Fig. 8. Image block constellation within the calibration room.

adjustment precision parameters in comparison to the spatial resection results. The imaging constellation of the nine used positions is shown in Fig. 8. Thereby the camera axes were oriented convergent in a way that a maximal number of object points are visible within the image.

In a first step, the bundle adjustment was calculated as a free network adjustment using the different geometric models for fisheye lenses as well as using the central perspective geometry for the purpose of comparison. The coordinates of 131 object points, the interior orientation of the lens-camera-combination and the exterior orientation of each image were determined. Additional parameters were not estimated in the first calculation. Table 3 shows the standard deviation of the unit weight as well as the average standard deviations of the estimated object point coordinates (RMS) as results of the calculations. It is obvious that the basic geometric model of the equisolid-angle projection is most suitable to describe the used lens. The precision in image space using this geometric model is 1.3 pixels. The precision in object space is 1–3 mm. The models of the orthographic, stereographic and central perspective projection deliver much worse results.

Afterwards the same calculations were processed again, but with consideration of all additional parameters (lens distortion, affinity, shear) (Table 4). It turns out that the additional parameters, in particular the parameters of the radial symmetric lens distortion are able to compensate the deviations between the geometric models of the equidistant, equisolid-angle and stereographic models completely, as the results from the calculation applying these models are almost identical. This confirms the conclusions which were drawn from the spatial resection results.

For each projection model the strongest correlation between the parameters of the basic model and the distortion model occurs between y_0 and B_2 (77%). All other correlation coefficients between the parameters of each basic projection model and the parameters of the distortion model are below 70%. Therefore correlations are rather uncritical concerning numerical instabilities in the bundle adjustment.

However, the resulting standard deviation of unit weight from the bundle block adjustment (0.3 pixels) is much worse than the values achieved by spatial resection (0.1 pixels). If the object point coordinates were the limiting factor for the accuracy of the results of the spatial resection, the calculation of a bundle adjustment without control points should produce better accuracies. This is not the case. A possible explanation for the inferior results of the bundle adjustment can be seen in a temporal instability of the interior orientation parameters, especially the principal point coordinates. To verify this assumption, the calculation of the bundle adjustment with the equisolid-angle projection model was carried out a second time, but with image variant interior orientation and additional parameters. This means, for each image individual values have been estimated. A parameterization as suggested in Maas (1998), where image variant parameters of the interior orientation but one single set of additional parameters for the whole image block are calculated, cannot be realized with the software used at this stage.

Table 5 lists the calculation results of the bundle adjustment and their standard deviation for each image. There are significant differences noticeable. The principal distance varies in the order of 20 μm, the principal point in x-direction by about 20 μm (≈2.5 pixels) and the principal point in y-direction even about 65 μm (≈8 pixels). These principle point variations have also been observed for digital still video cameras earlier (e.g. Maas and Niederöst (1997)). This confirms the need of introducing image variant interior orientation parameters for the used lens and camera combination.

The bundle adjustment with image variant interior orientation parameters results in a standard deviation of unit weight of

Table 5
Bundle adjustment results (principle distance and principal point) applying the equisolid-angle projection model with image variant interior orientation.

Image	Number of object points	Principal distance, c (mm)	Principal point	
			x_0 (mm)	y_0 (mm)
1	93	8.0176 ± 0.0048	-0.1608 ± 0.0032	-0.0574 ± 0.0032
2	91	8.0156 ± 0.0047	-0.1534 ± 0.0031	-0.0581 ± 0.0031
3	95	8.0089 ± 0.0040	-0.1516 ± 0.0024	-0.0594 ± 0.0031
4	103	8.0131 ± 0.0046	-0.1446 ± 0.0028	-0.0662 ± 0.0031
5	96	8.0257 ± 0.0048	-0.1512 ± 0.0027	-0.0811 ± 0.0031
6	96	8.0230 ± 0.0051	-0.1536 ± 0.0028	-0.0786 ± 0.0033
7	79	8.0151 ± 0.0039	-0.1476 ± 0.0017	-0.0216 ± 0.0020
8	108	8.0292 ± 0.0039	-0.1402 ± 0.0029	-0.0173 ± 0.0020
9	113	8.0249 ± 0.0041	-0.1481 ± 0.0029	-0.0153 ± 0.0020

Table 6
Bundle adjustment results (precision of 3D object coordinates) applying the equisolid-angle projection model with image variant interior orientation.

	Standard deviation of unit weight $\hat{\sigma}_0$	RMS_X	RMS_Y	RMS_Z
Equisolid angle model	0.111 pixel	2.32 mm	2.10 mm	3.98 mm

0.11 pixels, which is now equivalent to the standard deviation resulting from the spatial resection. However, the precision of the resulting object coordinates (Table 6) is clearly below the values resulting from the bundle adjustment with only one set of interior orientation and additional parameters (compare Table 4, 2nd row). The reason for the increase of the standard deviation of the object coordinates is the higher number of parameters which causes higher correlations between the parameters, in particular between object coordinates and interior orientation.

The similar standard deviation of unit weight allows for the conclusion that the accuracy of the control points used in the spatial resection did not pose a restriction on the accuracy of the calculation results. The necessity of the image variant interior orientation parameterization can not be generalized to the geometric fisheye models or to the use of fisheye lenses, as it can most probably be attributed to the stability of the camera body and the lens mount.

Finally the resulting point clouds were investigated for systematic effects. For this purpose the object coordinates resulting from the bundle adjustment applying the equisolid-angle projection model (with one set of interior orientation and additional parameters) were compared to the reference coordinates (see Section 3.1). The check point differences showed some systematic effects, which are probably caused by the instabilities of the interior orientation parameters. Similar systematic patterns have been reported in Grün et al. (1995). Comparing the 3D coordinates resulting from the bundle adjustment results with image variant interior orientation parameters to the reference coordinates, these systematic effects are reduced (about ca. 75%), but not fully removed. The pattern of the check point coordinate differences is identical or similar for the equisolid-angle, equidistant and stereographic projection model. It has to be noted, that the remaining systematic effects might partly also be attributed to the quality of the reference coordinates.

4. Conclusions

Despite some imaging quality degradations, fisheye lenses can be used in photogrammetric measurement tasks. Using proper geometric fisheye lens models, subpixel accuracy image measurements can be translated into 3D object space. Four different geometric fisheye lens models were implemented and verified on the basis of images taken by a 14 Mpix camera equipped with a Nikkor 8 mm fisheye lens: equidistant, equisolid-angle, orthographic and stereographic projection geometry. A spatial resection as well as a self-calibrating bundle adjustment with imagery taken in a special hemispherical camera calibration room both resulted in a standard deviation of unit weight of 1/10 pixel when inserting additional parameters for lens distortion.

It could be shown that there are large differences between the results using different basic geometric models, which can, however, largely be compensated applying a standard set of radial-symmetric lens distortion parameters to the fundamental equidistant, equisolid-angle and stereographic basic geometric model.

Using the basic geometric model extended by a standard polynomial correction approach for modeling the radial symmetric lens distortion is sufficient to achieve subpixel accuracy, which is satisfying for most applications of fisheye lenses compiled in the introduction of the paper. Introducing parameters for decentering lens distortion and for affinity and shear of the sensor did not improve the calibration results significantly.

As long as the radial symmetric lens distortion parameters are considered within the model the calibration accuracy is nearly independent of the chosen basic geometric model. However, in contrast to the calibration accuracies the parameter values differ strongly if different basic geometric models are applied. Therefore the individual calibration values are only valid in combination with the basic geometric model used for the calibration.

In practical applications of each fisheye lens, the most suitable geometric model should be used, which is sometimes known from the manufacturer's specifications. Otherwise, testing different models will likely unveil the correct model.

Furthermore it is recommended to use image variant interior orientation parameters within the bundle adjustment of fisheye imagery, as the calculation accuracy can be improved significantly.

References

Abraham, S., Förstner, W., 2005. Fish-eye-stereo calibration and epipolar rectification. ISPRS Journal of Photogrammetry and Remote Sensing 59 (5), 278–288.
Amiri Parian, J., 2007. Sensor modelling, terrestrial panoramic camera calibration and close-range photogrammetric network analysis. Ph.D. thesis, ETH Zürich.
Bakstein, H., Pajdla, T., 2002. Panoramic Mosaicing with a 180 Field of View Lens. In: Proc. IEEE Workshop on Omnidirectional Vision, Los Alamitos, US, June 2002, pp. 60–67.
Beers, B.J., 1997. 3-D landsurveying using the FRANK method: CycloMedia Mapper. In: Gruen, A., Kahmen, H. (Eds.), In: Proc. 4th Conference on Optical 3-D Measurement Techniques, Zurich, Switzerland, pp. 283–290.
Bonnet, G., 2004. SpheroCam – Full spherical panoramic camera and processing of panoramic image data. International archives of Photogrammetry, Remote Sensing and Spatial Information Sciences 34 (Part 5/W16), (on CD-ROM).
Brown, D., 1971. Close-Range Camera Calibration. Photogrammetric Engineering 37 (8), 855–866.
El-Hakim, S.F., 1986. Real-time image meteorology with ccd cameras. Photogrammetric Engineering and Remote Sensing 52 (11), 1757–1766.

Frank, O., Katz, R., Tisse, C.-L., Durrant-Whyte, H., 2007. Camera calibration for miniature, low-cost, wide-angle imaging systems. In: Proc. 18th British Machine Vision Conference, Warwick, UK, 10–13 September 2007, (on CD-ROM).

Gennery, D.B., 2006. Generalized camera calibration including fish-eye lenses. International Journal of Computer Vision 68 (3), 239–266.

Grün, A., Maas, H.-G., Keller, A., 1995. Kodak DCS200 — a camera for high accuracy measurements? In: El-Hakim, S. (Eds.), SPIE Proceedings Series 2598, pp. 52–59.

Kannala, J., Brandt, S.S., 2006. A generic camera model and calibration method for conventional, wide-angle, and fish-eye lenses. IEEE Transactions on Pattern Analysis and Machine Intelligence 28 (8), 1335–1340.

Luhmann, T., 2004. A historical review on panorama photogrammetry. International Archives of Photogrammetry, Remote Sensing and Spatial Information Sciences 34 (Part 5/W16), (on CD-ROM).

Luhmann, T., Hastedt, H., Tecklenburg, W., 2006. Modelling of chromatic aberration for high precision photogrammetry. International Archives of Photogrammetry, Remote Sensing and Spatial Information Sciences 36 (Part 5), 173–178.

Maas, H.-G., Niederöst, M., 1997. The accuracy potential of large format stillvideo cameras. In: El-Hakim, S. (Eds.), SPIE Proceedings Series 3174, pp. 145–152.

Maas, H.G., 1998. Ein Ansatz zur Selbstkalibrierung von Kameras mit instabiler innerer Orientierung. Publikationen der DGPF, 18. Wissenschaftlich-Technische Jahrestagung der DGPF, Munich, Germany, 14–16 October, pp. 47–53.

Orekhov, V., Abidi, B., Broaddus, C., Abidi, M., 2007. Universal camera calibration with automatic distortion model selection. In: Proc. IEEE International Conference on Image Processing 6, San Antonio, US, 16–19 September, pp. 397–400.

Prenzel, W.-D., 1986. Entwicklungstendenzen der fotografischen Optik. Bild und Ton – wissenschaftliche Zeitschrift für visuelle und auditive Medien 39 (1), 5–13.

Ray, S.F., 1994. Applied Photographic Optics – Lenses and Optical Systems for Photography, Film, Video and Electronic Imaging, second ed. Focal Press.

Regensburger, K., 1990. Photogrammetrie – Anwendungen in Wissenschaft und Technik, first ed. Verlag für Bauwesen, Berlin.

Scaramuzza, D., Martinelli, A., Siegwart, R., 2006. A toolbox for easily calibrating omnidirectional cameras. In: Proc. IEEE International Conference on Intelligent Robots and Systems, Beijing, China, 9–15 October, pp. 5695–5701.

Schneider, D., Schwalbe, E., 2005. Design and testing of mathematical models for a full-spherical camera on the basis of a rotating linear array sensor and a fisheye lens. In: Grün, A., Kahmen H. (Eds.), In: Proc. 7th Conference on Optical 3-D Measurement Techniques, Vienna, Austria, pp. 245–254.

Schneider, D., Maas, H.-G., 2006. A geometric model for linear-array-based terrestrial panoramic cameras. The Photogrammetric Record 21 (115), 198–210.

Schneider, D., Schwalbe, E., 2008. A geometric model for integrated processing of terrestrial laser scanner data and fisheye-camera image data. International archives of Photogrammetry. Remote Sensing and Spatial Information Sciences 37 (Part B5), 1037–1045.

Schröder, G., 1981. Technische Fotografie. Kamprath Reihe. Vogel Verlag, Würzburg.

Schwalbe, E., 2005. Geometric Modelling and calibration of fisheye lens camera systems. International Archives of Photogrammetry, Remote Sensing and Spatial Information Sciences 36 (Part 5/W8), (on CD-ROM).

Schwalbe, E., Maas, H.-G., Roscher, M., Wagner, S., 2006. Profile based sub-pixel-classification of hemispherical images for solar radiation analysis in forest ecosystems. International Archives of Photogrammetry, Remote Sensing and Spatial Information Sciences 36 (Part 7), (on CD-ROM).

Schwalbe, E., Maas, H.-G., 2006. Ein Ansatz zur Elimination der chromatischen Aberration bei der Modellierung und Kalibrierung von Fisheye-Aufnahmesystemen. In: Luhmann, T., Müller, C. (Eds.), Photogrammetrie, Laserscanning, Optische 3D-Messtechnik, Beiträge der Oldenburger 3D-Tage 2006, Oldenburg, Germany, February 2006, pp. 122–129.

van den Heuvel, F., Verwaal, R., Beers, B., 2006. Calibration of fisheye camera systems and the reduction of chromatic aberration. International Archives of Photogrammetry, Remote Sensing and Spatial Information Sciences 36 (Part 5), (on CD-ROM).

Wagner, S., 1998. Calibration of grey values of hemispherical photographs for image analysis. Agricultural and Forest Meteorology 90 (1/2), 103–117.